

# Spectroscopic properties, spatial and luminosity distributions of the UCM survey galaxies<sup>1</sup>

J. Gallego<sup>2</sup>

*Lick Observatory, University of California, Santa Cruz, CA 95064, USA; jgm@ucolick.org*

*Dpto Astrofísica, Universidad Complutense de Madrid, E-28040 Madrid, Spain*

J. Zamorano, M. Rego

*Dpto Astrofísica, Universidad Complutense de Madrid, E-28040 Madrid, Spain; jaz@ucmast.fis.ucm.es*

and

A.G. Vitores

*Dpto Astrofísica, Universidad Complutense de Madrid, E-28040 Madrid, Spain*

*EUIT Industrial. Universidad Politécnica, E-28012, Madrid, Spain*

## ABSTRACT

A spectroscopic analysis of the whole sample of H $\alpha$  Emission-Line Galaxies (ELGs) contained in the lists 1 & 2 of the Universidad Complutense de Madrid (UCM) objective-prism survey is presented. A significant fraction (59%) of star-forming galaxies with low ionization or high extinction properties has been found. This kind of ELG is only incompletely detected in the blue or in other ELG surveys. We have found evidence for evolution among some of the different ELG classes. A comparison between the populations detected by Case, Kiso, UM and UCM surveys is presented. We conclude that a deep H $\alpha$  survey is better able to sample all the ages, evolutionary stages and luminosities of current star-forming galaxies than other surveys using blue-emission lines or colors. Finally, the luminosity and spatial distributions of the UCM galaxies are determined. The contribution of the newly found current star-forming ELGs adds new clues to galaxy evolution and has to be taken into account when trying to consider the density of ELGs and total Star Formation Rate in the Universe.

*Subject headings:* galaxies: evolution, stellar content — galaxies: structure, surveys

---

<sup>1</sup>Partly based on observations collected at the German-Spanish Astronomical Center, Calar Alto, Spain, operated by the Max-Planck-Institute für Astronomie (MPIA), Heidelberg, jointly with the Spanish National Commission for Astronomy.

Partly based on observations made with the Isaac Newton Telescope operated on the island of La Palma by the Royal Greenwich Observatory in the Spanish Observatorio del Roque de Los Muchachos of the Instituto de Astrofísica de Canarias.

<sup>2</sup>del Amo UCM Foundation Fellow.

## 1. Introduction

The UCM objective-prism survey is being carried out with the main purposes of identifying and studying new star-forming galaxies and quantifying the properties of the Star Formation Rate (SFR) in the local universe. The technique used for detection is the presence of  $\text{H}\alpha + [\text{NII}] \lambda 6584$  emission at objective-prism Schmidt photographic plates. Because the specific details have already been summarized in the first and second lists (Zamorano *et al.* 1994; 1996) of our exploration, and the photometric aspects of the sample are presented in Vitores *et al.* (1996a and 1996b), we concentrate here in the spectroscopic characteristics of the survey. A companion study of the far-infrared properties of this sample of ELGs is published in Rego *et al.* (1993). Finally, the  $\text{H}\alpha$  luminosity function and the current SFR from a complete sample of the survey can be found in Gallego *et al.* (1995).

We have carried out a program for obtaining long-slit CCD spectroscopy of the whole lists 1 & 2 of the UCM survey. The main goals are (1) the selection characteristics, biases, and completeness limits of the sample, (2) the physical properties that are responsible for the spectroscopic behavior and (3) the spatial and luminosity distributions to determine how they compare with those of other ELGs surveys and normal galaxies. The spectroscopic data and individual classifications are available in Gallego *et al.* (1996), hereafter referred as Paper I.

Given the importance of the comparison between the results of such a survey in the red and others using different techniques for detecting ELGs we have also considered those surveys with a similar analysis available in the literature. As a representative sample of blue objective-prism surveys we have used the lists III and IV of the University of Michigan (UM) survey (Salzer 1989, Salzer *et al.* 1989a & Salzer *et al.* 1989b). For the surveys based in the blue excess we have used the subsample of Kiso Ultraviolet Galaxies (KUG) from Augarde *et al.* (1994) and Comte *et al.* (1994). Finally, as a mix of blue objective prism and blue excess we have used the Case survey for blue or emission-line galaxies (CG) from Rosenberg *et al.* (1994) and Salzer *et al.* (1995).

The current paper presents a discussion on the overall properties of the UCM galaxies. In section 2 we address the physical properties. In section 3 we focus on spatial distributions. The selection effects

are considered in section 4. Finally, we present a discussion about the luminosity function in section 5. A summary of our results and conclusions is given in section 6. Unless it is specified a value of  $H_0 = 50 \text{ km s}^{-1} \text{ Mpc}^{-1}$  was assumed.

## 2. Physical properties of the UCM emission-line galaxies

In order to classify the ELGs found by the UCM survey, we have adopted the scheme of Salzer *et al.* (1989a, 1989b). The reader is referred to paper I for a complete description of the various types. We have only considered the observationally well-defined Seyfert 1 (Sy 1) and Seyfert 2 (Sy 2) galaxies. Also were considered Starburst Nuclei (SBN). These are spiral galaxies that host a nucleus with an star-forming process. The  $\text{H}\alpha$  luminosity is greater than  $10^8 \text{ L}_\odot$  and present red colors. Any emission line present in the blue are faint due to extinction. The Dwarf Amorphous Nuclear Starburst (DANS) are similar to the SBN but at lower scale. They are spectroscopically indistinguishable from SBNs, but their  $\text{H}\alpha$  luminosities are lower than  $5 \cdot 10^7 \text{ L}_\odot$ . The HII Hotspot class (HIIH) includes all those bright galaxies with a global star-forming process and an optical spectrum dominated by blue colors and strong emission lines. Their  $\text{H}\alpha$  luminosities are similar to those of SBN class. The Dwarf HII Hotspot (DHIIH) galaxies have spectroscopic properties similar to those of HIIH class except  $\text{H}\alpha$  luminosities lower than  $5 \cdot 10^7 \text{ L}_\odot$ . Finally, the Blue Compact Dwarfs (BCD) are characterized by  $\text{H}\alpha$  luminosities  $\leq 5 \cdot 10^7 \text{ L}_\odot$ , strong emission lines and equivalent widths (EW) of several hundred angstroms. Giant Irregular, Magellanic Irregular and Interacting Pair classes were not considered because these types rely mainly on morphological aspects of the candidate.

### 2.1. Overall spectroscopic properties

Some spectroscopic and physical properties for each of the UCM ELGs types are presented in tables 1 and 2. Table 1 lists the mean values and standard deviations of the  $[\text{OIII}] \lambda 5007/\text{H}\beta$ ,  $[\text{NII}] \lambda 6584/\text{H}\alpha$ ,  $[\text{OII}] \lambda 3727/\text{H}\beta$ , and  $[\text{OI}] \lambda 6300/\text{H}\alpha$  emission-line ratios. The last column gives the number of ELGs. Table 2 lists the mean values of several fundamental parameters. The composition of the sample by types is 14 Seyfert galaxies (8%), 111 red ELGs (SBN and DANS, 59%) and 61 blue HII-spectrum ELGs (i.e.

HIIH, DHIIH and BCD, 33%). It is worth noting that meanwhile the UM survey contains 11% and the Case survey 18% of SBN galaxies, the UCM survey is detecting 44%. Since SBN have weak lines in the blue, all this population of star-forming galaxies is being poorly considered by surveys in that spectral region. Lewis (1981) called them WOR (Weak Oxygen Red) galaxies. Salzer *et al.* (1989) includes only five objects in the SBN class for the UM survey. However, almost all of the  $\text{H}\alpha$  luminosity observed in the UCM survey at bright absolute-magnitudes is hosted in the form of SBNs (Gallego *et al.* 1995, Coziol 1996). Salzer *et al.* (1989a) claim that the UM survey would recover all the SBNs by the [OII]  $\lambda 3727$  line, but 38 SBN of the UCM survey do not present any [OII] in emission and the mean EW is only 12 Å (27 Å when considering only the 45 with [OII] detected). Because the contrast limits for both UM and UCM surveys are 10 Å, the completeness when using this line can not be assured for the SBN class. The CFRS survey (Tresse *et al.* 1996) has also found a considerable 38% of SBN galaxies in a field sample up to  $z=0.3$ .

The DANS galaxies are also poorly sampled by the UM survey (a total of 15 objects in list III and IV,  $0.04 \square^{-1}$ ) but are well represented in both Case (37 objects,  $0.20 \square^{-1}$ ) and UCM (28 objects,  $0.08 \square^{-1}$ ) samples. They present almost identical characteristics no matter the survey considered, with weak lines in the blue, average  $M_B=-18.4$  and  $\text{EW}([\text{OIII}]) \lesssim 10$  Å. For the UCM sample we obtain an average  $\text{EW}(\text{H}\alpha)=54$  Å and average colors of  $B-V=0.38$  and  $V-R=0.28$  with  $E_{B-V}=0.55$ . These properties point to reddened low-ionization objects easily found by the  $\text{H}\alpha+[\text{NII}]$  emission but only detectable by the [OII]  $\lambda 3727$  line (38 Å mean value for the UCM) at the blue-excess or blue emission-line surveys. The mean  $\text{H}\alpha$  luminosity obtained for the DANS UCM subsample is only  $0.58 10^8 L_\odot$  but, as it will be seen in the next section, present ELGs surveys could be missing a large fraction of such objects.

It is worth noting that the BCDs in the UCM survey are in average an absolute magnitude brighter than those found by UM and Case surveys. BCDs are characterized by faint absolute magnitudes and large equivalent widths, with the largest values for the lowest absolute magnitudes. The apparent magnitude limit of the UCM survey is close to  $r=18$  (Vitores *et al.* 1996b), instead of the 19.5 apparent magnitude for the UM survey. Even at very low redshift, galaxies with absolute magnitudes below -16 would

appear fainter than the UCM limit value (for  $z=0.01$  and  $M_r=-15.5$  it results an apparent magnitude of  $r=18.5$ ). In fact, the UCM survey presents a lack of sensitivity for low luminosity objects, detecting only the brightest members of the BCD class, i.e., those with EW less extreme (The faintest object is UCM1612+1309, with  $M_r=-16.7$ ). Furthermore, the average  $\text{EW}([\text{OIII}])$  for the UM, UCM and Case BCD subsamples are 1090, 458 and 247 Å, confirming that the UCM value is biased by its lower sensitivity to faint absolute magnitude and large EW objects.

## 2.2. Line-ratio and ionization diagrams

In Figure 1 has been represented the [NII]/ $\text{H}\alpha$  versus [OIII]/ $\text{H}\beta$  diagnostic diagram (Veilleux & Osterbrock 1987) for the UCM sample. As expected, all the ELGs classes are positioned following a narrow sequence defined by the HII models. It starts at the upper-left corner of the diagram for the high-ionization low-metallicity BCDs, and it ends at the lower-right corner for the low-ionization and high-metallicity objects.

The low ionization corner is well populated by the UCM galaxies. In comparison with the UM survey, the UCM survey is recovering a higher fraction of low ionization galaxies. The comparison is not straightforward for the Kiso and Case samples because only a relatively small number of galaxies from both surveys were observed spectroscopically in the  $\text{H}\alpha$  region.

The low-ionization population is also present in the Figure 2. It plots the logarithm of the [OIII]/ $\text{H}\beta$  ratio (the excitation parameter) against absolute magnitude  $M_B$ . As a complement for the UCM sample we have added the eleven objects found by Boroson *et al.* (1993, hereafter referred as BST) in a search for extremely low-luminosity objects using  $\text{H}\alpha$  and narrow-band filters at the KPNO 0.9m telescope. This completes the low-luminosity end of the  $\text{H}\alpha$ -selected sample.

ELG's spectrum is the result of the physical properties and the importance of the on-going starburst relative to the underlying population. Based in time scale arguments, Salzer *et al.* (1995) pointed out that there should be a large population of low-ionization dwarf galaxies which starburst is already after the peak in luminosity and that is not well detected by the UM or any other existing survey. These objects would show a soft spectrum with weak emission lines and small EWs. According to the models (Leitherer

& Heckman 1995, Stasinska & Leitherer 1996), if we let a starburst evolve several Myr, they move along the HII sequence to the lower-right corner in Figure 1, but to the lower-left in Figure 2, out of the HII sequence. The properties of the pure burst remain almost constant until the 10Myr step, when the O stars begin to disappear, a drop happens in all physical properties and the object presents a weaker emission-line spectrum.  $M_B$  becomes 1-2 magnitudes fainter,  $\Delta(V-R) \sim 0.4$  mag and  $\text{EW}(\text{H}\alpha)$  drops by a factor of ten. Detection techniques based in blue colors or  $\text{H}\alpha$  emission (as Case or UCM surveys), have advantage over those using high-ionization lines (as UM survey) when detecting these soft-spectrum galaxies. A fraction of such a population is actually being recovered in the form of DANS objects. At Figure 2 these objects have been oversized for better recognition. They are low-ionization ELGs, with low EWs and a lower  $M_B$  than the expected value from the HII sequence. All these magnitudes are coherent with a past-the-peak stage. Furthermore, the parental population for DANS galaxies would be ELGs with higher ionization features and larger EWs, when the ionizing stars have a higher mean effective temperature. This pre-DANS population can be found among the HIIH and DHIIH ELGs, whose physical properties are the expected.

In Figure 3 the ionization diagram ( $\log([\text{OIII}]/\text{H}\beta)$  versus  $\log([\text{OII}]/[\text{OIII}])$ ) for the UM, KUG, UCM and Case galaxies is shown. The models from Stasinska & Leitherer (1996) are plotted for different metallicities and the whole range of ionization parameters. High ionization is in the upper-left and low ionization is in the lower-right. As expected, only some of the possibilities are populated by ELGs. At the high ionization region all the samples except the KUG one are well represented. Only Case and UCM present galaxies than deviate from the HII sequence, being mainly in the low-ionization region.

For explaining the better ability of the UCM survey to recover all kind of star-forming galaxies we have to rely on the nature of the tracer used by each survey. Since it is directly related to the number of massive stars, the  $\text{H}\alpha$  luminosity is a direct measurement of current SFR. It is better than other optical Balmer lines like  $\text{H}\beta$ —affected by stellar absorption and reddening and with smaller photon flux—. Metallic nebular lines like  $[\text{OII}]$ ,  $[\text{OIII}]$ —affected by excitation and metallicity— IRAS fluxes (affected by the dust abundance and properties) or broad-band luminosity densities—dependent of stellar libraries for

calibration and very sensitive to the underlying stellar population—are more star-formation indicators than quantitative measurements (see, eg., Gallagher *et al.* 1989 and Kennicutt, 1992). These considerations imply that the best way to trace and quantify current star formation processes in the whole range of physical properties is by using an  $\text{H}\alpha$ -based detection technique. As a  $\text{H}\alpha$ -selected sample, the UCM sample populates almost all the regions of the ionization diagram.

### 2.3. Emission-line equivalent widths

We present in Table 3 and in Figure 4 the distribution in  $[\text{OIII}]$  EWs for the UCM sample, the Kiso data from Comte *et al.* (1994), and the UM data from Salzer *et al.* (1989a). The same data for  $\text{H}\beta$  EWs can be found in Table 4.

A total of 44% of UCMs do not present  $[\text{OIII}]$  at all, whereas 19% present EWs greater than 100 Å (age of a pure starburst below 5 Myr). The KUG sample has also a high fraction of no  $[\text{OIII}]$  galaxies (34%) but only has a 5% of objects above the 100 Å limit.

The UM sample is so rich in objects with large EWs that the mean value of the is almost 100 Å. The fraction of ELGs with no line is very low (4%), because this survey detects the candidates mainly by the presence of this line. Again the UM sample seems to be more biased to high ionization objects, missing a significative fraction of low-ionization star-forming galaxies. The reason why the Kiso sample does not detect large numbers of high-EW objects remains unclear. It may be due to a bright value in the apparent magnitude limit or to a selection effect in the subsample considered by Comte *et al.* (1994).

Because of its mixed blue excess and blue emission-lines selection nature, the Case survey should detect the full range of EWs. Now in Figure 5 the  $[\text{OIII}]$  EW histograms are plotted in a different way. A rectangle delimits the position of the first and third quartile and the mean value is also marked. Finally the whole range covered is delimited by a line. The mean and third quartile for Case and UCM samples agree pretty well, meanwhile the UM sample is centered at higher values.

Finally, one of the most fundamental parameters for characterizing the population of UCM ELGs is the distribution according to the  $\text{EW}(\text{H}\alpha+[\text{NII}])$  (Figure 6).

The mean value reaches 102 Å, with 35% of the

objects above this value. In the high-EW end there are three objects (UCM0056+0044, UCM1331+2901 and UCM1612+1309) with values over 400 Å. In the low-EW end only 15 objects (8%) are below 20 Å. Meanwhile no values over 1000 Å are set by the roles of the hottest plausible O-star continua and significant nebular continuum, it is clear that below the 10 Å limit the sensitivity of the survey decreases steeply. The wide range covered in the distribution points out that the H $\alpha$  technique is able to detect star-forming galaxies in an universal way.

#### 2.4. Abundances of the UCM galaxies

In order to estimate the metallicities of the UCM galaxies, we contrasted the emission-line ratios available for 125 UCM galaxies with the Stasinska & Leitherer (1996) stellar evolutionary synthesis code and single-zone gas (spherical symmetry, uniform chemical composition and density distribution) nebular photo-ionization code (Stasinska 1990). The results are summarized in Table 5. For each class it is given the number of components within the different metallicities considered, the total number and the mean metallicity in logarithmic (the solar abundance corresponds to 8.82) and natural solar units.

The redder SBN and DANS classes are more metallic than the bluer HIIH, DHIIH and BCDs (as expected from the self-enrichment by the current starburst episode if they correspond to a more evolved stage). We should find extremely metal-poor galaxies between the subsample of objects classified as BCDs. However, we also would expect to observe low metallicities at the low-ionization dwarfs discussed before. Perhaps the presence of two DANS with 1/10  $Z_{\odot}$  points to this possibility but more metallicities of objects similar to a4.483 are needed.

We also carried out high signal-to-noise spectrophotometry for a subsample of 15 UCM galaxies. The procedure followed is step-by-step described by Pagel *et al.* (1992). The average error for the electronic temperature is 5%. Considering the problem of the primordial Helium, when the electronic temperature was available and the He line fluxes were accurate enough (within a 10% error), also the Helium abundance was estimated. In Table 6 we give the electronic density as computed from the [SII] lines, the electronic temperature, the Oxygen abundance, the Oxygen to Nitrogen ratio, the ionic O $^{++}$ /Ne $^{++}$  and S $^{+}$ /H $^{+}$  ratios and finally the Helium abundance. Using these values, the metallicities estimated from the

models are correct within a 25%. None of the galaxies found have lower metallicities than 1/20  $Z_{\odot}$ . The reasons are mainly two. The first one is that it could be expected that, if galaxies with very low metallicities exist, they have very low luminosities, so only a ultra-deep survey would find them. The second one is a self-contamination problem (Kunth & Sargent 1986). There must be young massive O and B stars for having the emission-line spectrum used for computing the abundances. But these stars have strong winds that inject higher metallicity material in the interstellar medium. If so, the lowest abundances would be found at the neutral gas out of the already contaminated HII region surrounding the ionizing stars. This hypothesis seems to be confirmed by Kunth *et al.* (1994).

### 3. Spatial distribution of the UCM galaxies

#### 3.1. Pie diagrams and clustering

We utilized the CfA data (Huchra, Geller, Corwin 1995 and references therein) for the redshifts of all galaxies previously known at the regions covered by the UCM survey. A total of 4219 CfA galaxies and 196 UCM ELGs have been plotted in Figure 7. The declination dimension was suppressed.

The top panel corresponds to a highly clustered region centered at  $\alpha=15^{\text{h}}$  (UCM list 2). It includes the Coma (R.A. $\sim 13^{\text{h}}$ ) and the Hercules clusters (R.A. $\sim 16^{\text{h}}$ ). The bottom panel corresponds to a region of moderate density of field galaxies centered at  $\alpha=0^{\text{h}}$  (UCM list 1). Whereas in the Coma cluster there is a large number of H $\alpha$  emission-line galaxies it is worth noting that none of the Hercules galaxies were detected. We leave here this question open but perhaps it would be interesting a deeper study in H $\alpha$  of this cluster.

In Figure 8 a projection on the sky with all the galaxies that belong to the Coma cluster is shown. A total of 18 UCM ELGs inside Coma were not previously known, suggesting that perhaps our actual knowledge of the Coma population is not so complete. In fact three of each four are DANS or SBN and consequently reddened galaxies. How many of these galaxies remain undiscovered at Coma is a question being only slowly resolved (see for example Caldwell *et al.* 1996). The two-point correlation function for both all cluster (above, dots) and UCM samples (below, open symbols) are also plotted. The UCM galaxies (i.e., the star-forming galaxies) at the Coma cluster are less clustered than the galaxies of the cluster as a

whole. This picture suggests the idea that the star-formation inside clusters is indirectly modulated by the density of the intergalactic medium.

#### 4. Completeness of the UCM survey

In any survey for detecting emission-line features in objective-prism plates the apparent magnitude is not the only factor that contributes to the selection of a candidate.

##### 4.1. Total flux of the line+continuum feature.

Any candidate needs a total flux in the H $\alpha$ +[NII] region over a threshold value in order to be registered by the plate emulsion. The total flux and the equivalent width are two fundamental parameters for defining the selection criteria.

In the Figure 9 both parameters are plotted for the UCM sample. It can be observed a trend of larger EWs for fainter ELGs. According to the continuum decreases the line flux has to increase in order to maintain the line+continuum over the threshold value. The fundamental parameter of detectability is this total flux. In case of an universal population of galaxies all the regions in Figure 9 might be occupied. In our Figure there are empty regions. Is very easy that a near-saturation continuum masks any possible emission (lower-left corner). As an example the object NGC7677 is a 13.9<sup>m</sup> nearby galaxy with well-known emission-lines. However, this galaxy presents a completely saturated spectrum with no detectable emission. At lower-right corner are the faint galaxies with small EWs. Also the Surface brightness becomes important when the spectrum is near the saturation limit. If the total luminosity of the candidate is spread across a larger area it will be easier to notify the possible emission present. Conversely, low-surface brightness galaxies will be lost if no bright emitting knot is present.

##### 4.2. Contrast of the emission line over the continuum.

Stronger emission lines make detection easier. There is a threshold value of  $\sim 10$  Å below which no objects are detected (see Figure 10). Only two galaxies were selected with lower EW values. The first was a miss-selection of an edge-on galaxy with a superimposed star (UCM2320+2428, 7 Å) and the second is a diffuse low surface-brightness galaxy (UCM2249+2149, 4 Å). An (x) marks the position this object and of a 8.196

(not detected because of its faintness although the EW is 84 Å). Several galaxies with confirmed emission, but with no emission feature in the objective-prism plates are labeled by crosses (+).

Because of the wavelength cut-off of the photographic emulsion, there is an upper limit in redshift at  $0.045 \pm 0.005$ . Since this cut-off is not completely sharp, objects with strong emission are detected at little higher redshifts (threshold  $\sim 30$  Å at  $z=0.04$ ). The variable dispersion of the prism, very important in the blue, is negligible in the H $\alpha$  region.

#### 5. Luminosity function of the UCM galaxies

For comparison purposes we have computed the luminosity function in a similar way that Salzer (1989) did for the UM survey. This author applies the original V/Vmax method (Schmidt 1968, Huchra & Sargent 1973) but considering a synthetic magnitude for the total flux of line+continuum ( $F_{L+C}$  in  $\text{erg s}^{-1} \text{cm}^{-2}$ ) at the Schmidt plate instead the normal apparent magnitude. This arbitrary magnitude is a function given by:

$$m_{L+C} = -17.0 - 2.5 \log (F_{L+C})$$

where the total  $F_{L+C}$  line+continuum apparent flux comes from

$$F_{L+C} = F_L \left( 1 + \frac{2PR}{EW} \right)$$

where  $F_L$  is the line flux and EW is the equivalent width (both measured in the spectra), P is the reciprocal dispersion of the objective prism and R is the spectral resolution (1950 Å mm $^{-1}$  and  $\sim 10\mu\text{m}$  respectively). The quantity V/Vmax results

$$\frac{V}{V_{max}} = \left( \frac{r}{r^*} \right)^3 = 10^{0.6(m - m^*)}$$

The subsample of 176 UCM galaxies with  $m_{L+C}$  brighter than 17.3 that makes  $\langle V/V_{max} \rangle = 1/2$  and  $\text{EW}(\text{H}\alpha + \text{[NII]}) > 10$  Å was considered as complete and representative for the UCM galaxies. The  $m_{L+C} \leq 17.3$  limit corresponds to a line+continuum flux of  $1.9 \times 10^{-14} \text{ erg s}^{-1} \text{cm}^{-2}$ . Below this value the sample presents larger incompleteness.

Now the classical approach (Huchra & Sargent 1973) was followed for this sample. First, the value of Vmax is obtained from

$$V_{max} = \frac{4}{3} \pi 10^{0.6(m^* - M - 25.0)}$$

where  $m^*=17.3$  and  $M$  is the absolute magnitude corresponding to the synthetic magnitude and computed with the known redshifts and  $H_o=75 \text{ km s}^{-1} \text{ Mpc}^{-1}$ . The Schmidt estimator is then given by

$$\phi(M) = \frac{4\pi}{\Omega} \sum_i \left( \frac{1}{V_{max}^i} \right)$$

where the summation is over all galaxies with blue absolute magnitude in the interval  $M_B \pm 0.5$  and  $\Omega$  is the solid angle in steradians covered by the survey. We choose  $H_o=75$  and the blue absolute magnitude in order to compare our results with the other surveys previously analyzed. The final luminosity function for the UCM and the published values for BST, UM, Kiso and Case (UV-excess-selected only) galaxies are listed in Table 7.

The table gives  $\log \phi(M)$  (galaxies per unit magnitude interval per  $\text{Mpc}^3$ ) and the number of galaxies included in each magnitude bin. The same luminosity functions are displayed in Figure 11. The errors bars plotted represent the square root of the number of galaxies in each absolute magnitude. Symbols with no error bars associated correspond to intervals which contain only one galaxy. In the upper-left corner have been plotted BST (open diamonds) and UCM (filled circles) luminosity functions together for a global  $\text{H}\alpha$ -selected sample.

We adopted a classical Schechter function (Schechter 1976) as given by Felten (1977) where the free parameters are  $\phi^*$ ,  $M^*$  and  $\alpha$ . The  $\alpha$  corresponds to the slope of low-luminosity end, whereas  $\phi^*$  and  $M^*$  give the position of the turning point. The best fit to the data is given in Table 8.

The luminosity functions reflect what we have already pointed out in previous sections. The low-luminosity end is poorly sampled by the UCM survey due to the bright apparent magnitude limit. In any case, the study of Boroson *et al.* (1993) becomes the perfect complement for the UCM survey data, coinciding at the common bin of -18. Joining the two samples, the resulting luminosity function for  $\text{H}\alpha$  emission-line galaxies is the more accurate measurement of the luminosity distribution of current star-forming galaxies. This situation for  $\text{H}\alpha$  versus other lines is analogous to that in galactic nuclei, where both AGN and star formation are more often detectable at  $\text{H}\alpha$  than in the blue (see for example Heckman 1980 or Keel 1983). It is worth noting that  $\phi^*$  for the total  $\text{H}\alpha$  ELGs sample is larger than the Case value and twice the UM value. The total density of

ELGs rises from  $\sum \log \phi(M) = -1.51$  for the UM ELGs to  $\sum \log \phi(M) = -1.15$ . When comparing this value with the obtained from field luminosity functions, the  $\text{H}\alpha$  ELGs would amount for 0.07 galaxies per cubic Mpc, i.e., for  $\sim 15\%$  of all galaxies over the luminosity range considered.

## 6. Summary and conclusions

We present the spectroscopic properties, spatial distribution and luminosity function for the sample of  $\text{H}\alpha$  ELGs from the lists 1 & 2 of the UCM survey. We have found a large fraction (59%) of low-ionization or high-extinction star-forming galaxies. These objects are poorly sampled by other surveys in the blue since they do not present blue colors or strong emission lines. However, as these galaxies are current star-formers, they have to be taken into account when considering the SFR in any volume of Universe surveyed.

We have found evidences for evolution between the different ELGs classes considered. The DANS objects seem to be the past-the peak stage for the HIIH and DHIIH classes. Several arguments including total luminosity, equivalent widths and colors favor this hypothesis. The extension of these objects towards low luminosities predicts a population of low ionization and luminosity ELGs very difficult to trace. The population of extremely-faint  $\text{H}\alpha$  emission-line galaxies found by BST can be considered as a probe of such population. If even the UCM, UM or Case surveys are tracing these galaxies not properly is because there are strong selection effects. In fact, the Case survey detects several low-ionization candidates using the blue color-excess, the UM detects those with higher ionization and the UCM a mixing of both types. We have estimated average abundances for every ELG class. Accurate spectrophotometric abundances for several objects confirm (within 25% error) these results. No galaxy with metallicity below  $1/20 Z_\odot$  have been found.

Because the UCM galaxies are selected by their  $\text{H}\alpha$  emission and this feature is the best tracer for current SFR, we tried to compare the distribution of the UCM and CfA samples in order to obtain new clues about the effect of the intergalactic environment in the triggering of the starburst processes. The sample covers both regions with low and high density of galaxies. In the Coma field,  $\text{H}\alpha$  ELGs are considerably less clustered than the normal population. This result

points to a dependence of the SFR with the galaxy density. A total amount of 18 not previously known constituents were discovered in this well-studied cluster by means of their H $\alpha$  emission. Also quite interesting is that no one H $\alpha$  ELG has been detected in the Hercules cluster.

The parameters that determine the selection of an object by the UCM survey are the total line+continuum flux and the equivalent width of H $\alpha$ +[NII]. The UCM sample seems to be poorly sampling low-luminosity galaxies. The poor information for the low end of the luminosity function was completed after considering the analysis optimized for these objects by Boroson *et al.* (1993). As a global result, the H $\alpha$  selection method is better able to detect galaxies at any level of star-forming activity than previous surveys. The total density of ELGs rise to 0.07 galaxies per cubic Mpc, i.e., roughly the 15% of all galaxies over the luminosity range considered and almost twice the value obtained by Salzer (1989) for the UM survey.

This work was supported in part by the Spanish "Programa Sectorial de Promoción del Conocimiento" under grants PB89-124 and PB93-456. JG acknowledges the partial financial support from NASA grant GO-05994.01-94A. He is grateful to D. C. Koo and R. Guzmán for their hospitality at Lick Observatory, UCSC.

## REFERENCES

Augarde, R., Chalabaev, A., Comte, G., Kunth, D., & Maehara, H., 1994, A&AS 104, 259.

Boroson, T.A., Salzer, J.J., Trotter, A., 1993, (BST) ApJ 412, 524.

Caldwell, N., Rose, J.A., Franx, M., Leonardi, A., 1996, AJ 111, 78.

Comte, G., Augarde, R., Chalabaev, A., Kunth, D., & Maehara, H., 1994, A&A 285, 1.

Coziol, R., 1996, A&A 309, 345.

Dopita, M.A. & Evans, I.N., 1986, ApJ 307, 431.

Felten, J.E., 1977, AJ 82, 861.

Gallagher, J.S., Bushouse, H., Hunter, D.A., 1989, AJ 97, 700.

Gallego, J., Zamorano, J., Aragón-Salamanca, A., & Rego, M., 1995, ApJ 455, L1.

Gallego, J., Zamorano, J., Rego, M., Alonso, O., Vitores, A.G., 1996, (Paper I) A&AS in press.

Heckman, T.M., 1980, A&A 87, 142.

Huchra, J., Sargent, W.L.W., 1973, ApJ 186, 433.

Huchra, J.P., Geller, M.J., Corwin, H.G.J., 1995, ApJS 99, 391.

Kennicutt, R.C., 1992, ApJ, 388, 310.

Keel, W.C., 1983, ApJ 269, 466.

Kunth, D., Sargent, W.L.W., 1986, ApJ 300, 496.

Kunth, D., Lequeux, J., Sargent, W.L.W., Viallefond, F., 1994, A&A 282, 709.

Leitherer, C., Heckman, T.M., 1995, ApJS 96, 9.

Lewis, D.L., 1981, Ph.D. thesis, University of Michigan.

Pagel, B.E.J., Simonson, E.A., Terlevich, R.J., Edmunds, M.G., 1992, MNRAS, 255, 325.

Rego, M., Cordero-Gracia, M., Zamorano, J., Gallego, J., 1993, AJ 105, 427.

Rosenberg, J.L., Salzer, J.J., 1994, AJ 108, 1557.

Salzer, J.J., 1989, ApJ 347, 152.

Salzer, J.J., MacAlpine, G.M., Boroson, T.A., 1989a, ApJS 70, 447.

Salzer, J.J., MacAlpine, G.M., Boroson, T.A., 1989b, ApJS 70, 479.

Salzer, J.J., Moody, J.W., Rosenberg, J.L., Gregory, S.A., and Newberry, M.V., 1995, AJ 109, 2376.

Schechter, P.L., 1976, ApJ 203, 297.

Schmidt, M., 1968, ApJ 151, 393.

Stasinska, G., 1990, A&A 83, 501.

Stasinska, Leitherer, 1996, ApJ in press.

Tresse, L., Rola, C., Hammer, F., Stasinska, G., Le Fevre, O., Lilly, S., and Crampton, D., 1996, MNRAS in press.

Veilleux, S. & Osterbrock, D.E., 1987, ApJS 63, 295.

Vitores, A.G., Zamorano, J., Rego, M., Alonso, O., Gallego, J., 1996a, A&AS 118, 7.

Vitores, A.G., Zamorano, J., Rego, M., Gallego, J., Alonso, O., 1996b, A&AS in press.

Zamorano, J., Rego, M., Gallego, J., Vitores, A.G., González-Riestra, R., Rodriguez-Caderot, G., 1994, ApJS 95, 387 (UCM list 1).

Zamorano, J., Gallego J., Rego, M., Vitores, A.G., Alonso, O., 1996, ApJS 105, 343 (UCM list 2).

TABLE 1  
AVERAGE LINE RATIOS FOR THE UCM GALAXIES

Type	[OIII]/H $\beta$	$\sigma$	[NII]/H $\alpha$	$\sigma$	[OII]/H $\beta$	$\sigma$	[OI]/H $\alpha$	$\sigma$	N
Sy 1	1.1	0.3	0.3	0.2	1.7	1.8	0.01	0.00	5
Sy 2	11.4	5.3	1.5	1.1	11.0	7.9	0.20	0.20	9
SBN	1.5	1.1	0.5	0.2	4.8	3.5	0.10	0.10	83
DANS	1.6	1.1	0.4	0.1	4.4	2.9	0.03	0.01	28
HIIH	3.3	1.3	0.2	0.1	4.5	3.5	0.03	0.02	40
DHIIH	4.0	1.0	0.2	0.05	5.3	2.8	0.04	0.02	14
BCD	6.6	1.0	0.05	0.02	1.9	0.9	0.02	0.01	7

TABLE 2  
AVERAGE PHYSICAL PARAMETERS

Type	M <sub>r</sub>	L <sub>H<math>\alpha</math></sub> (10 <sup>8</sup> L <sub>⊙</sub> )	z	H $\alpha$	Equivalent width (Å)			E <sub>B-V</sub>	B-V	V-R
				H $\alpha$	H $\beta$	[OII]	[OIII]			
Sy 1	-21.3	5.22	0.0334	260	51	13	38	0.463	0.10	0.26
Sy 2	-22.0	3.78	0.0342	86	9	26	90	0.794	0.47	0.56
SBN	-21.1	2.24	0.0281	77	9	27	11	0.789	0.30	0.30
DANS	-20.3	0.58	0.0243	54	9	38	13	0.547	0.38	0.28
HIIH	-20.4	2.32	0.0240	150	24	63	74	0.514	0.04	0.06
DHIIH	-19.1	0.38	0.0226	107	17	64	78	0.360	0.03	0.01
BCD	-18.1	0.35	0.0226	294	72	89	458	0.096	-0.07	-0.09

TABLE 3  
[OIII] EW DISTRIBUTIONS

	UCM	KUG	UM
Total	145	105	139
No [OIII]	64 (44%)	36 (34%)	6 (4%)
< 10 Å	47 (32%)	35 (33%)	21 (15%)
> 50 Å	42 (29%)	23 (22%)	81 (58%)
> 100 Å	26 (19%)	5 (5%)	61 (44%)
> 400 Å	5 (3%)	0 (0%)	23 (16%)

TABLE 4  
H $\beta$  EW DISTRIBUTIONS

	UCM	KUG	UM
Total	218	117	139
No H $\beta$	35 (16%)	...	6 (4%)
< 10 Å	120 (55%)	57 (49%)	31 (22%)
> 40 Å	22 (10%)	2 (2%)	41 (29%)
> 50 Å	15 (7%)	1 (1%)	33 (24%)

TABLE 5  
DISTRIBUTION OF THE DIFFERENT ELG CLASSES ACCORDING TO METALLICITIES AND THEIR MEAN VALUES

Type	B Z $_{\odot}$	C Z $_{\odot}/2$	D Z $_{\odot}/5$	E Z $_{\odot}/10$	F Z $_{\odot}/20$	No total	Z/Z $_{\odot}$ mean	Z $_{\odot}/Z$ mean	log([O/H])+12 mean
SBN	23	35	3	0	0	61	0.67	1.5	8.65
DANS	6	11	0	2	0	19	0.62	1.6	8.61
HIIH	5	8	19	3	0	35	0.37	2.7	8.39
DHIIH	0	0	2	11	1	14	0.11	9.0	7.87
BCD	0	0	0	3	3	6	0.075	13.0	7.71

TABLE 6  
ACCURATE ABUNDANCES FOR SELECTED UCM GALAXIES

UCM	$N_e$ ( $\text{cm}^{-3}$ )	$T_e$ ( $10^3$ K)	$^{12+\log(\text{O/H})}$	O/N	$\text{O}^{++}/\text{Ne}^{++}$	$\text{S}^+/\text{H}^+$	Y
UCM0049-0006	100	15.5	7.76	0.60	0.79	5.36	0.265
UCM0049+0017	100	16.1	7.59	0.60	0.79	5.83	0.271
UCM0050+0005	30	13.1	8.10	1.25	0.58	5.86	0.254
UCM0056+0044	75	14.7	7.79	1.16	0.77	5.70	0.310
UCM0150+2032	200	10.0	8.22	1.08	0.63	5.90	0.248
UCM0156+2410	100	10.0	7.97	0.66	0.30	5.80	
UCM1324+2926	120	14.5	7.86	1.21	0.70	5.70	0.295
UCM1331+2901	100	15.2	7.88	1.21	0.78	5.07	0.252
UCM1429+2645	30	16.5	7.80	0.83	0.75	5.83	
UCM1612+1309	110	14.3	7.99	0.04	0.70	5.60	0.333
UCM2251+2405	200	9.9	7.94	0.55	0.77	6.10	
UCM2304+1640	100	13.9	8.01	1.66	0.64	5.68	0.244
UCM2316+2028	100	10.0	8.01		0.85		
UCM2326+2435	10	13.1	8.03	1.33	0.74	5.65	0.308
UCM2327+2515	180	14.7	7.90	1.21	0.49	5.77	

TABLE 7  
LUMINOSITY FUNCTIONS FOR ALL THE FOUR ELGs SURVEYS

$M_B$	UCM ELGs		BST ELGs		UM ELGs		KUG ELGs		Case	
	$\log\phi(M_B)$	N	$\log\phi(M_B)$	N	$\log\phi(M_B)$	N	$\log\phi(M_B)$	N	$\log\phi(M_B)$	N
-23.0	0.00	0	0.00	0	0.00	0	0.00	0	0.00	0
-22.0	-4.46	8	0.00	0	-6.03	1	-5.66	5	-5.59	1
-21.0	-3.13	32	0.00	0	-4.60	8	-4.58	15	-4.30	5
-20.0	-2.78	51	0.00	0	-3.85	17	-3.69	29	-3.28	21
-19.0	-2.80	40	0.00	0	-2.77	23	-3.08	30	-2.57	27
-18.0	-2.74	14	-2.79	1	-2.94	24	-3.12	7	-2.37	10
-17.0	-2.43	7	0.00	0	-2.88	15	-2.74	4	-1.92	9
-16.0	-3.43	1	0.00	0	-1.76	21	-2.06	5	-1.79	4
-15.0	-3.29	1	-1.57	5	-2.15	7	-1.65	3	-1.15	2
-14.0	0.00	0	-1.72	2	-2.67	4	0.00	0	-1.06	1
-13.0	0.00	0	-1.82	1	-2.43	2	0.00	0	0.00	0

TABLE 8  
SCHECHTER FUNCTIONS FOR ALL THE FOUR ELGs SURVEYS

	UCM	BST	UM	KUG	Case
$M^*$	-20.4	...	-19.45	...	-20.05
$\alpha$	-0.90	~-1.3	-1.20	...	-1.21
$\phi^*$	0.0033	<0.007	0.0012	...	0.0022

Fig. 1.— Line diagnostic diagram plotting [OIII]  $\lambda 5007/\text{H}\beta$  against [NII]  $\lambda 6584/\text{H}\alpha$  both in logarithmic scale. The different symbols indicate the ELG class (see text).

Fig. 2.— Excitation versus absolute magnitude for the UCM galaxies. The different symbols indicate the ELG class. They have been also plotted the  $\text{H}\alpha$  selected ELGs found by Boroson *et al.* (1993).

Fig. 3.— Excitation versus [OII]/[OIII] ratio. The symbols are the same as for Figure 1.

Fig. 4.— Histogram of the [OIII]  $\lambda 5007$  EW in logarithmic scale for the UCM, KUG and UM galaxies.

Fig. 5.— Mean values, first quartiles and extreme values for the [OIII] EWs at Case, UM, Kiso and UCM samples.

Fig. 6.— Histogram of the  $\text{H}\alpha+[\text{NII}]$  EW in logarithmic scale for the UCM galaxies.

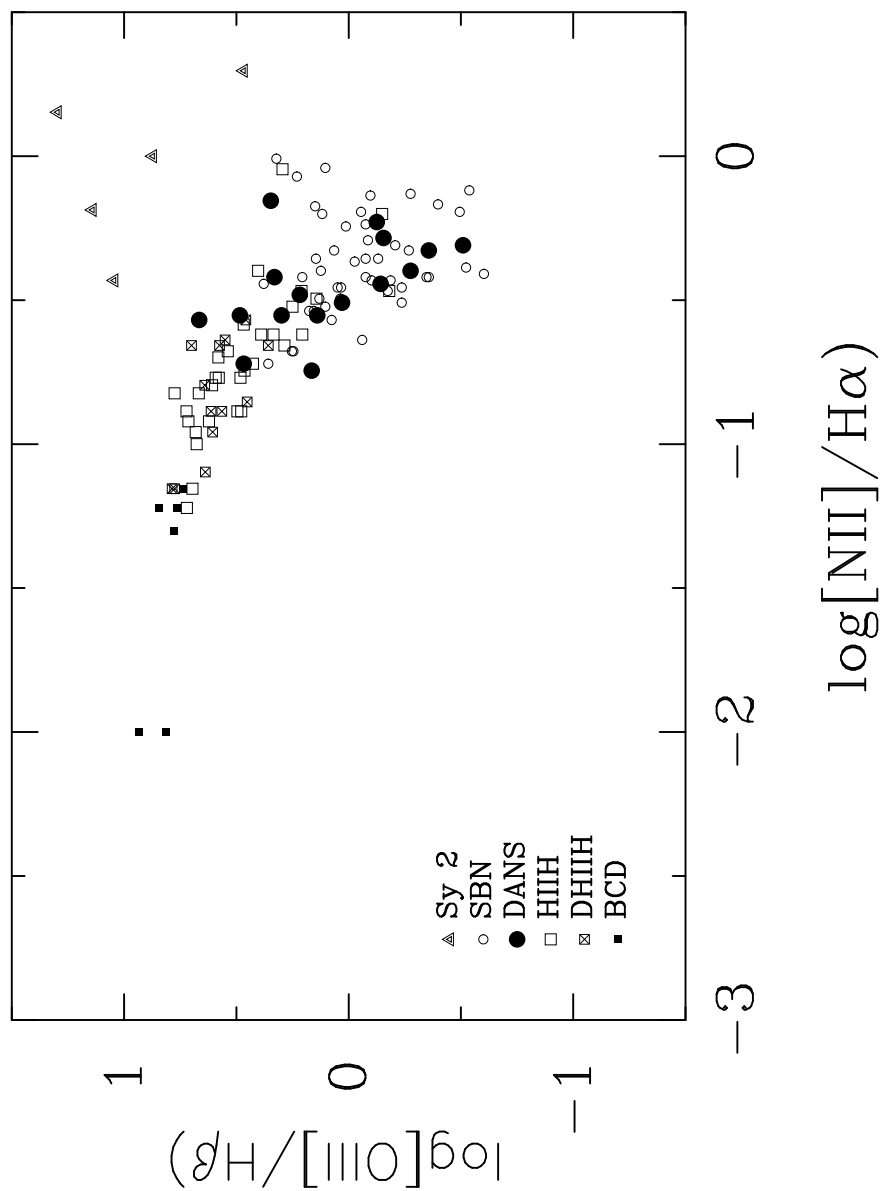
Fig. 7.— Spatial distribution for CfA (dots) and UCM (open circles) galaxies.

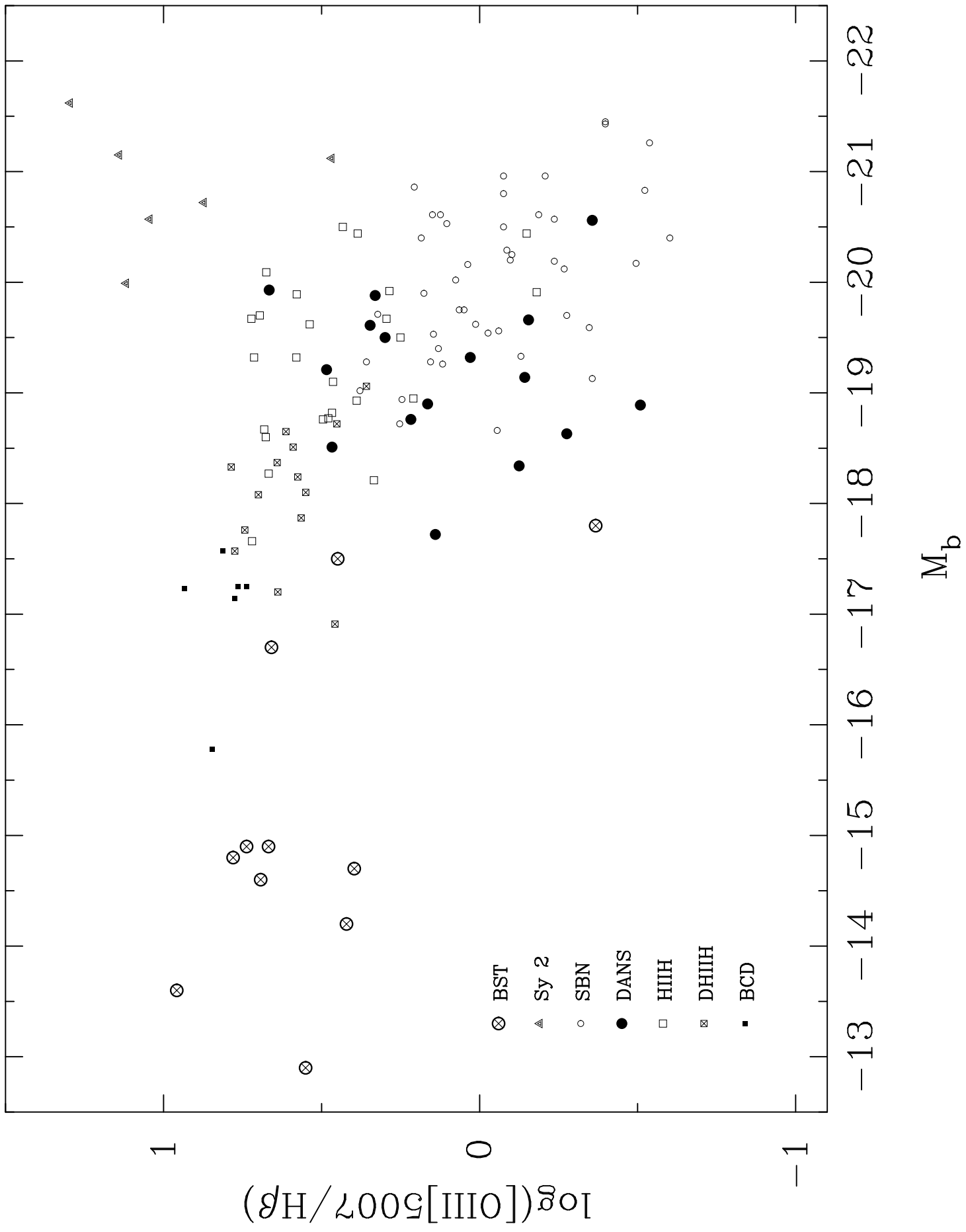
Fig. 8.— Angular correlation function for Coma galaxies and UCM galaxies in the cluster.

Fig. 9.— Logarithm of the  $\text{H}\alpha+[\text{NII}]$  equivalent width versus  $r$  apparent magnitude. The lack of faint galaxies with low EWs is clear (see text).

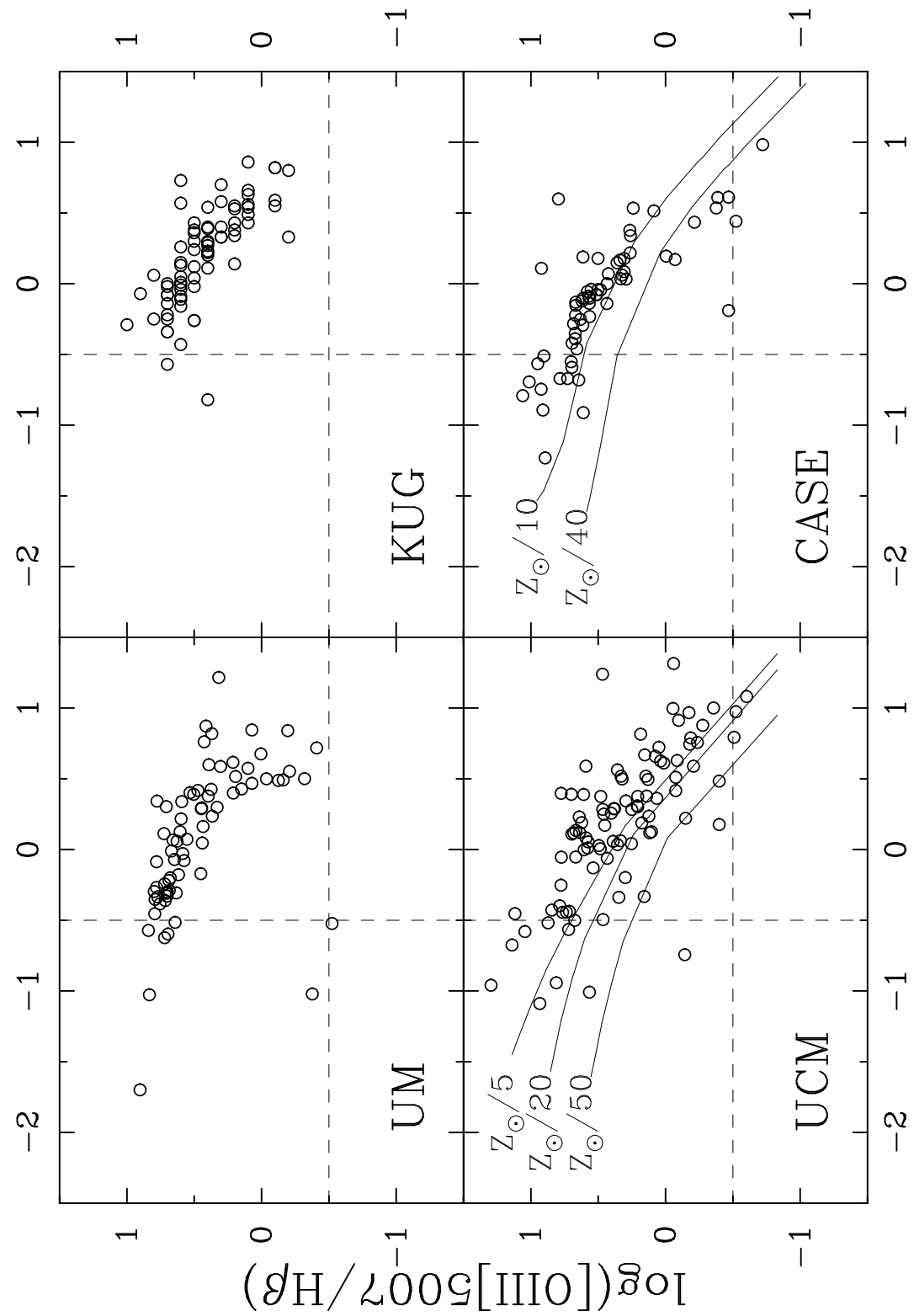
Fig. 10.— Logarithm of the  $\text{H}\alpha+[\text{NII}]$  equivalent width versus redshift. An asp correspond to the object a8.196. Other objects with small emission but not detected are plotted as crosses.

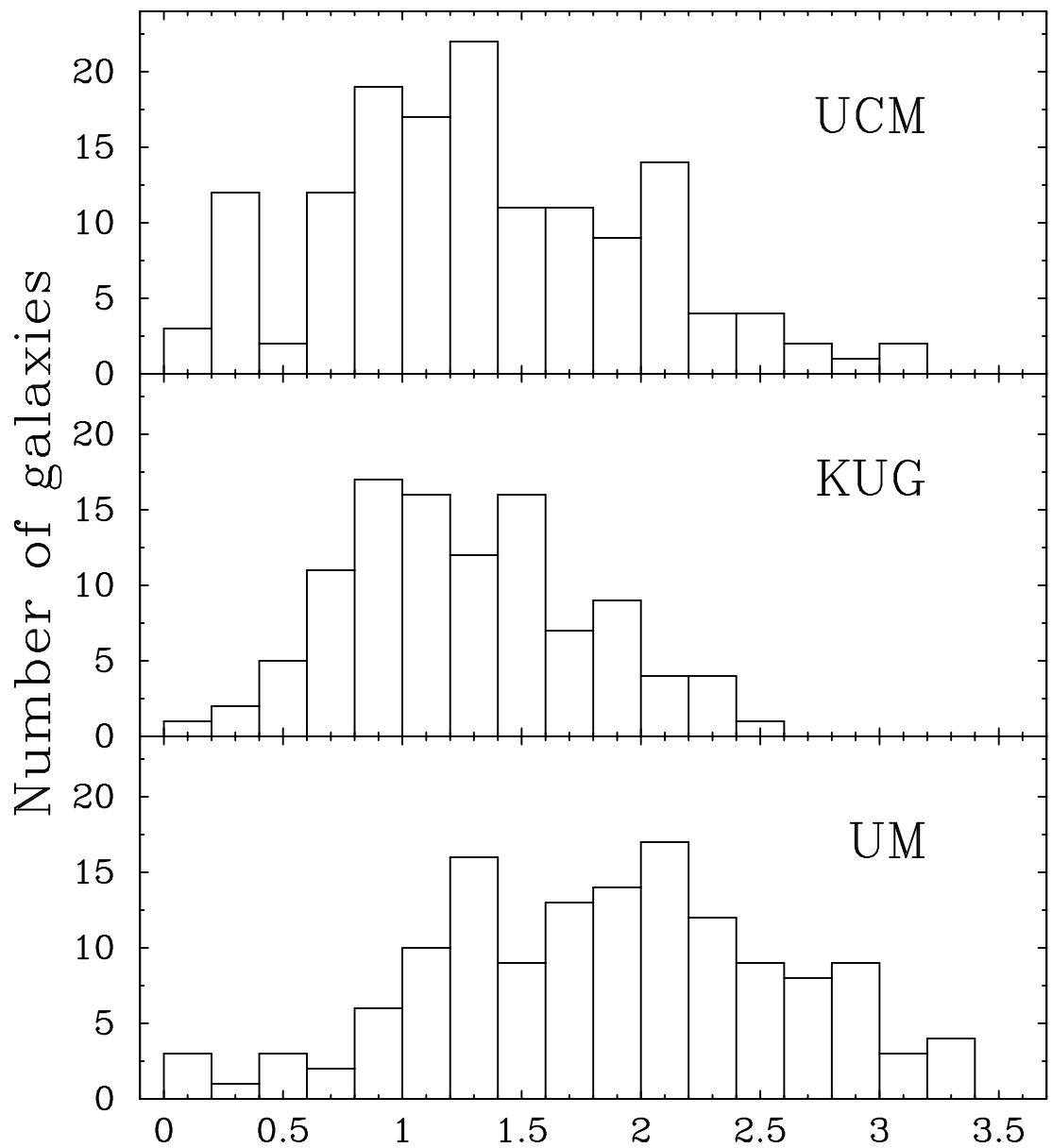
Fig. 11.— Luminosity functions for the different ELGs surveys.





$\log([\text{OII}]3727/\text{[OIII]}5007)$





log EW([OIII]λ5007)

